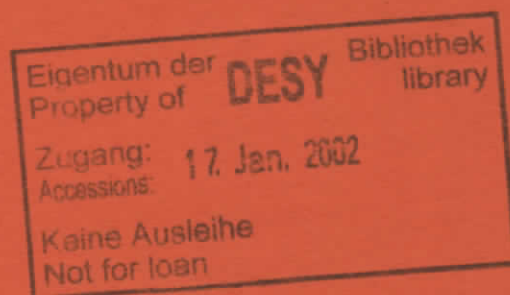


DESY SR 89-08

December 1989



The Asymmetric Wiggler at HASYLAB

J. Pfüger, G. Heintze

Hamburger Synchrotronstrahlungslabor HASYLAB at DESY, Hamburg

ISSN 0723-7979

NOTKESTRASSE 85 · 2 HAMBURG 52

DESY behält sich alle Rechte für den Fall der Schutzrechtserteilung und für die wirtschaftliche Verwertung der in diesem Bericht enthaltenen Informationen vor.

DESY reserves all rights for commercial use of information included in this report, especially in case of filing application for or grant of patents.

To be sure that your preprints are promptly included in the
HIGH ENERGY PHYSICS INDEX ,
send them to the following address (if possible by air mail) :

DESY
Bibliothek
Notkestrasse 85
2 Hamburg 52
Germany

DESY SR 89-08
December 1989

The Asymmetric Wiggler at HASYLAB

J. Pflüger and G. Heintze
Hamburger Synchrotronstrahlungslabor HASYLAB at DESY,
Notkestr. 85, D-2000 Hamburg 52, West Germany

Abstract

An asymmetric wiggler for the production of intense circularly polarized X-rays has been designed and tested successfully at HASYLAB. The device has ten periods and a period length of 240 mm. The magnetic design, device parameters and the results of magnetic field measurements are described. In order to characterize the circular polarization of the emitted light, the results of an experiment using this device for spin dependent photoabsorption at the Gd and Pt L_3 edges in Gd metal and in an Pt Fe alloy are presented.

to be published in: Nucl. Instr. Meth.

ISSN 0723-7979

Introduction

During the last decade, insertion devices (ID's) were developed and came widely into use as intense sources of synchrotron radiation (SR). It is well known that intensities which exceed those obtained from dipole magnets up to several orders of magnitude can be obtained. Conventional ID's like the existing wiggler W1 at HASYLAB which is in operation since 1984 produce a sinusoidally varying field. The emitted light is linearly polarized in the observation plane and is used from the XUV- to the X-ray region [1].

However, especially in the X-ray region, there are a number of experiments which need circularly polarized light. Examples are: elastic magnetic scattering, magnetic surface scattering, spin dependent photoabsorption, magnetic Compton scattering or inelastic magnetic X-ray scattering. Since all the above mentioned techniques deal with very small cross sections, they need high incident fluxes of circularly polarized photons.

Several special ID's have been proposed to produce circularly polarized photons [2-5]. Some of them have already been tested in prototypes, some are still under construction. In the X-ray region up to 20 keV even in high energy machines like DORIS II only the helical wiggler of Yamamoto and Kitamura [3] which has already been tested at the Photon Factory [6] and the asymmetric wiggler of Goulon et al. [5] are of practical interest. The mechanical requirements of an asymmetric wiggler are much simpler as compared to the helical wiggler which needs two crossed independent magnet structures that circumbuild the electron beam. The drive mechanics and the support structure of an asymmetric wiggler are identical to those needed for a symmetric sinusoidal one which makes its implementation on an existing drive mechanics straightforward.

There is an increasing demand for intense circularly polarized x-rays at HASYLAB too. We therefore decided to set up an asymmetric wiggler in order to have such an intense polarized photon source available. The principle of the asymmetric wiggler has not been verified experimentally up to now. Therefore we could gain first experience in the design and performance of such a device. This experience is also very useful for a considerably larger device planned for DORIS III [7].

The Magnetic Structure

The principle of the asymmetric magnet structure is illustrated in Fig. 1. Pure NdFeB blocks are arranged in such a way that strong short positive poles are surrounded by two negative and correspondingly weaker poles. The whole magnet structure resembles an array of one period wigglers and airspaces in between the modules where the weak poles are formed by the half-poles. The field integral of this device along the electron orbit should be of course zero, since the magnetization of the magnet blocks in the vertical direction cancels out to zero. This magnetic arrangement is more effective in producing the desired asymmetric fields than that proposed by Goulon et al. [5]. The same principle like ours, but instead using the more sophisticated hybrid technology, was proposed by Barthès et al. [8], a prototype of which is under construction at LURE [9].

The magnet blocks are mounted on holders with a dovetail support. In this way the airspace between the magnetic modules can be changed. Presently a period length of 240 mm and an airspace of 80 mm is used. Magnet dimensions are 40 x 40 x 90 mm for the full blocks. The remanent field of the magnets is 1.2 Tesla. Presently 10 periods are mounted on 2.4 m long girders made of magnetic steel, but magnets for three more periods are available which can be mounted by reducing the airspace correspondingly.

We decided not to set up a completely new beamline but instead use that of the already existing W1 wiggler. The girders of the asymmetric wiggler were therefore equipped with flanges that were compatible to flanges on the girders and the drive mechanics of the already existing W1 wiggler. Thus it is possible to exchange the complete magnet structures and provide circularly polarized photons on this beamline. By a suitable choice of the magnet dimensions it was possible to match the width of the emitted light cone to that of the W1 structure.

It is now straightforward to exchange the magnetic structures. Our first experience shows that an exchange (asymmetric to symmetric or vice versa) needs less than one hour.

Magnetic Measurements

The magnetic field of the asymmetric magnet structure on the symmetry axis as a function of the coordinate along the electron orbit is shown in the upper part of Fig. 2. The magnetic gap was 34 mm. These data were taken with a 3-D measuring bench in combination with a Hall-probe system. The linearity of the Hall-probe was better than 10^{-3} , the absolute precision of the motion control was better than ± 0.1 mm in all three directions. By a suitable computer controlled stepping motor drive "on the fly" measurements with a typical rate of 25 measurements per second were made. A scan over 3 m like that shown in Fig. 2 with a measuring interval of 1 mm takes two minutes. A peak field of 0.82 Tesla ± 1.3 % is observed for the strong positive poles, while -0.54 Tesla ± 1.3 % was found for the weak negative poles. The field in the middle of the airspace was measured to be -0.07 Tesla ± 0.8 %. It can be changed by changing the airspace correspondingly. The first and second field integral I_1 and I_2 defined as

$$I_1(x) = \int_{-\infty}^x B_y(x') dx' \quad (1)$$

$$I_2(x) = \int_{-\infty}^x I_1(x') dx' = \int_{-\infty}^x \int_{-\infty}^{x'} B_y(x'') dx'' dx' \quad (2)$$

are also shown in Fig. 2. I_1 is proportional to the angular deflection Θ_e of the e^- -beam, I_2 proportional to the orbital displacement z . The exact relationship is given by:

$$\Theta_e \text{ [mrad]} = (5.866 \times 10^5 / \gamma) \cdot I_1 \text{ [T}\cdot\text{m]} \quad (3)$$

$$z \text{ [mm]} = (5.866 \times 10^5 / \gamma) \cdot I_2 \text{ [T}\cdot\text{m}^2] \quad (4)$$

where γ is the kinetic energy of the electrons in units of the rest mass energy. For DORIS operated at 5.3 GeV ($\gamma = 10371$), a maximum deflection angle of ± 1.2 mrad is observed which corresponds to a K-value of 12.3 while the oscillating amplitude is only about 80 μm which is a factor of 25 less than the standard deviation of the horizontal e^- -beam size at the W1 site. From the value of I_1 well behind the magnet structure, it is seen that the field integral is already very close to zero. In order to have vanishing

influence on the stored e^- -beam outside the wiggler, a 2.5 m long precision coil in connection with a precision electronic integrator was used. An exact zero value was obtained by using several shims of 0.5 mm thick iron. However, even without these shims, the deviation from zero was small.

Emission Characteristics

A parametric plot of the magnetic field against the first field integral or equivalently using eq. (3), the electron beam deflection angle Θ_e is very illustrative since it shows the magnetic fields that contribute to the emission in a given horizontal direction. Figure 3 shows such a parametric plot for the central period. This plot has the form of a kidney which is typical for an asymmetric device. For a symmetric sinusoidal one this curve would look like an ellipse.

The incoherent emission of a wiggler can be calculated in the bend source approximation where no distinction between the horizontal observation angle Θ_H and the electron beam deflection angle Θ_e is made. The emission of the wiggler is thus analyzed in terms of bending magnet sources. The strengths and signs of the fields for a given $\Theta = \Theta_H = \Theta_e$ are looked up in the $B(\Theta)$ curve. For Θ_H larger than the maximum deflection angle, the calculated intensity is zero. The $B(\Theta)$ curve can be derived from calculated as well as from measured data like those in Fig. 3. In this way the inclusion of measured data is straightforward. The horizontally and vertically polarized brightness functions I_H , I_L are calculated by using the formulae for dipole magnet radiation [10]. The four vector components of the Stokes vector are then readily calculated [11,12,13]

$$\begin{aligned} S_0 &= I_H + I_L &= I_R + I_L \\ S_1 &= I_H - I_L \\ S_2 &= 0 \\ S_3 &= \pm 2 \sqrt{I_H \cdot I_L} &= I_R - I_L \end{aligned}$$

Here R and L stand for right and left handed polarization, respectively.

$S_2 = 0$ since the phase of the horizontal and vertical amplitude is always $\pi/2$. The sign of S_3 is positive for positive field and positive vertical

observation angle, Θ_v or negative field and negative Θ_v . Otherwise S_3 is negative [10].

The Stokes vector components resulting from incoherent emission of the two points in a period contributing at a fixed Θ are simply the sum of the individual Stokes vector components.

The resulting circular polarization is readily calculated from the added Stokes vector components:

$$P_{\text{cir}} = S'_3 / S'_0$$

where the primes denote the summation over the two field points.

Figures 4-6 show calculated emission properties at a photon energy of 10 keV as a function of the horizontal and vertical observation angle when DORIS is operated at 5.3 GeV. The $B(\Theta)$ data of Fig. 3 were used for the calculation. The electron beam divergence is assumed to be zero. All three figures cover the same angular range from -0.2 to +0.2 mrad vertically and from -1.5 to 1.5 mrad horizontally. Figure 4 shows the angular distribution of the total intensity ($I'_R + I'_L$) in arbitrary units. A characteristic double peak structure is observed which is typical for an asymmetric device. Around ± 0.7 mrad two field values of similar magnitude but opposite sign contribute to the emission in that direction which is therefore stronger than at $\Theta_H = 0$ where practically only the positive pole contributes while the weak negative pole has vanishing intensity at 10 keV. For the same reasons therefore the two peaks contain only few polarized photons whereas the central region around $\Theta_H = 0$ below or above the horizontal plane contains most. For a direct comparison fig. 5 shows the angular distribution of polarized brightness ($I'_R - I'_L$) in arbitrary units. On comparing Figs. 4 and 5 it is evident that for an experiment using the asymmetric wiggler, a properly chosen aperture should be used in order to keep off the unpolarized photons that are emitted at larger horizontal angles.

Figure 6 shows the angular distribution of the degree of circular polarization of the emitted radiation defined as $(I'_R - I'_L) / (I'_R + I'_L)$ which might be an interesting figure of merit for some experiments.

Measurements of the emitted light

For the first measurements on the asymmetric magnet structure, an experiment using spin dependent photoabsorption, also called circular dichroism [14,15], was set up on the existing W1 beamline to analyze the polarization of the emitted radiation. This experiment is an absorption experiment where the absorber is a magnetic material. With the help of a magnetization coil the direction of the magnetization of the sample can be reversed. When circularly polarized light is used, different absorption spectra are measured depending on whether the magnetic moments are aligned parallel or antiparallel to the photon spin. Especially near the L_3 absorption edges this difference may be as large as several percent. We concentrated on the Gd L_3 edge of Gd metal at 7.243 eV and the Pt L_3 edge of an PtFe alloy at 11.564 keV. The circular dichroism of the samples was precisely known from earlier measurements on a bending magnet source.

To illustrate the experimental set-up, Fig. 7 shows a schematic drawing of this beamline. The light emitted by the asymmetric wiggler is monochromatized in the X-ray monochromator (XM). The first mirror (M) is not used. A focusing mirror (FM) focuses the monochromatized light onto the sample position. In front of the monochromator an aperture (SL) is installed which is adjustable in the horizontal and vertical direction. It can be moved in the whole observation plane so that the flux through it can be measured as a function of horizontal and vertical angle of its center. The full experiment will be discussed in much more detail in a further publication [16]. Fig. 8 shows the total flux through an 2x1 mm aperture (horizontal/vertical) as a function of the horizontal angle. The photon energy was 7.243 keV. The intensity was measured at the sample position with an ionization chamber. The open circles represent measured values. The full line is a calculation using the measured magnetic field and the geometry of the experiment. The electron beam divergence was properly taken into account. The calculations are normalized relative to the maximum of the experimental curves. Due to the limited width of the monochromator crystal of 50 mm, the measurement is cut off at larger horizontal angles. The double peak structure which was already seen in Fig. 4 is clearly visible.

Fig. 9 shows a vertical polarization profile measured at the Pt- L_3 edge at 11.564 keV. The polarization below the orbital plane is shown. Since we were

interested in quite large vertical angles and since the available vertical aperture was limited, the beam position center was chosen to be at the upper limit of the aperture. The open circles represent measurements and the full line represents the corresponding calculation. It is seen that the polarization starts from zero and tends towards a saturation value of 1 on going to larger vertical angles. We emphasize that we verified also the change of sign of polarization when crossing the orbital plane. Also typical error bars are given for the polarization. The main error is caused by the e⁻-beam stability which led to changes of the observation angle (see below).

Fig. 10 shows a horizontal scan at the Gd L_3 edge at 7.243 keV with a 3.3 x 1 mm aperture at a fixed vertical angle of 0.16 mrad below the orbital plane. Experiment and calculation differ more than in Fig. 9 but it is seen clearly that the polarization is highest at $\Theta_H = 0$ and decreases on going to larger horizontal angles just as it is suggested by Fig. 6. The two peaks in the total intensity scan in Fig. 8 which was taken at the same energy are not seen in the polarization curve in Fig. 10. This shows that the two peaks in Fig. 8 are only weakly polarized. Instead of error bars we reproduce calculations for a vertical angle of 0.16 mrad (full line), 0.14 mrad (dot-dashed line) and 0.18 mrad (dotted line). The different values correspond to changes in the observation angle caused by vertical electron beam position errors of +/- 0.5 mm. It is seen that the measurements lie fully within the range covered by these calculation.

In general, the measurements of both the total intensities and the polarization gave results that are fully consistent with the expected behavior.

Summary

A prototype of a new insertion device with an asymmetric field was built and tested for the first time. Its period length is 240 mm with an airspace of 80 mm which can be varied easily. Ten periods are presently installed. At a gap of 34 mm a peak field of 0.82 Tesla is observed. The K-parameter was determined to be 12.7.

The emitted radiation was characterized using spin dependent photoabsorption. All the results obtained were fully consistent with the expected

values. We thus believe that this device is a promising new source of intense circularly polarized X-rays.

Acknowledgement

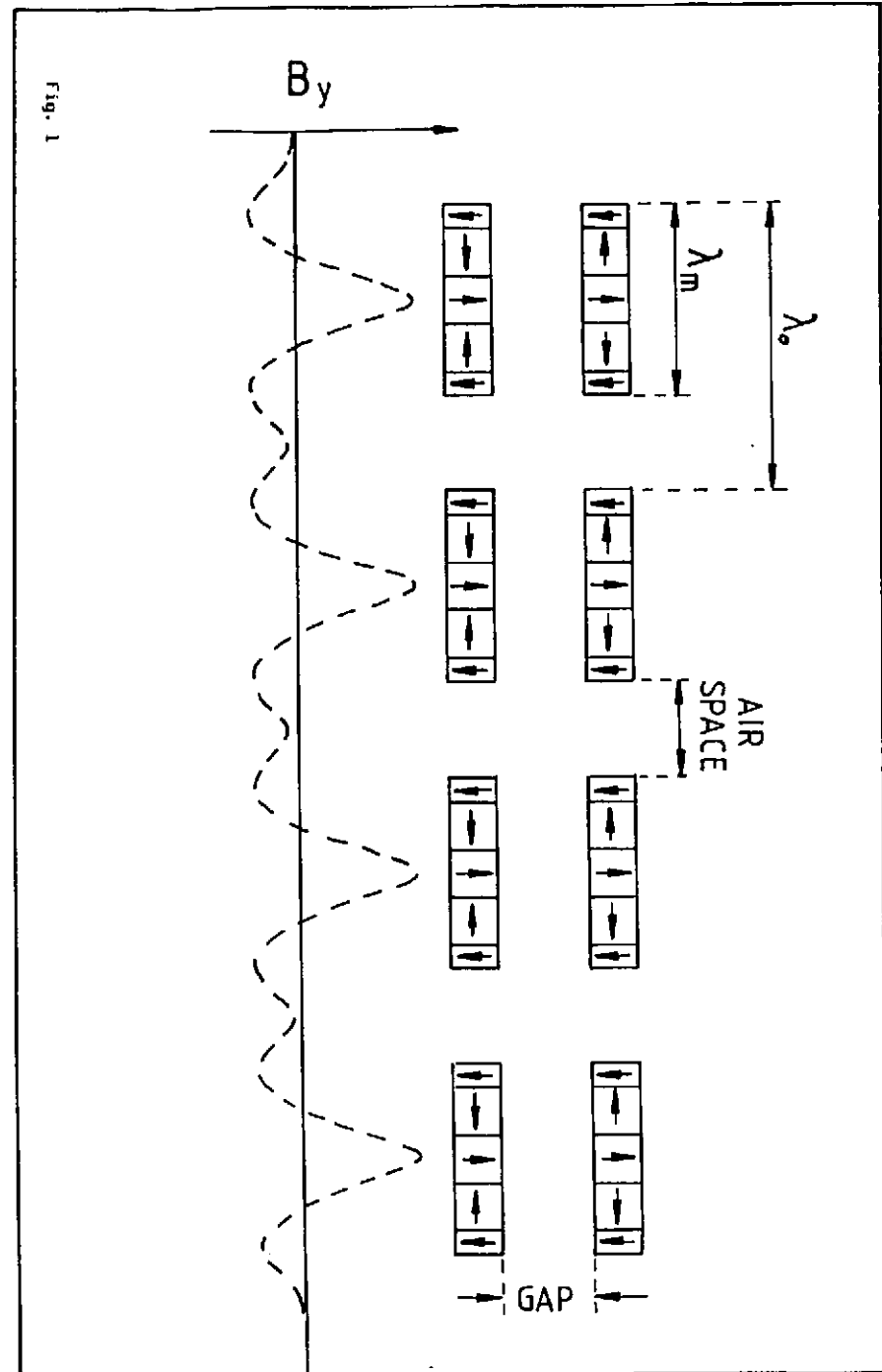
We thank R. Wienke and W. Wilhelm for the cooperation and for allowing us to use some of their results prior to publication.

References

- 1 P. Gürtler, A. Jackson, Nucl. Instr. and Meth. 208, 163 (1983);
P. Gürtler, Nucl. Instr. and Meth. A246, 91 (1986).
- 2 H. Onuki, Nucl. Instr. and Meth. A246, 94 (1986);
H. Onuki, N. Saito, T. Saito, App. Phys. Lett. 52, 173 (1988).
- 3 S. Yamamoto, H. Kitamura, Japn. Jour. of Appl. Phys. 26, L1613 (1987).
- 4 M.B. Moiseev, M.M. Nikitin, N.I. Fedosov, Izvestiya, Vysshikh Uchebnykh Zavedenii, Fizika 3, 76 (1978); Sov. Phys. J. 21, 332 (1978);
K.J. Kim, Nucl. Instr. and Meth. 222, 11 (1984).
- 5 J. Goulon, P. Elleaume, D. Raoux, Nucl. Instr. and Meth. A254, 192 (1987).
- 6 S. Yamamoto, H. Kawata, H. Kitamura, M. Ando, N. Saki, N. Shiotani, Phys. Rev. Lett. 62, 23 (1989).
- 7 J. Pflüger, P. Gürtler, to be published in Nucl. Instr. and Meth.
- 8 M. Barthés, C. Bazin, M.E. Couprie, A. Dael, C. Evesque, G. Humbert, Proc. of the 10th International Conf. on Magnet Technology, Boston, 21.-25. Sept. 1987.
- 9 D. Raoux, private communication
- 10 Koch, E.E., Ed.
Handbook of Synchrotron Radiation Vol. 1A, Amsterdam: North Holland Publishing Corporation, 1983
- 11 See for example "Synchrotron Radiation" ed. by C. Kunz, Topics in Current Physics Vol. 10, Springer Verlag, 1979
- 12 M. Born, E. Wolf, Principles of Optics, Pergamon Press, New York, 1980
- 13 B.A. Robson, The Theory of Polarisation Phenomena, Clarendon Press, Oxford, 1974
- 14 G. Schütz, R. Wienke, W. Wilhelm, W. Wagner, P. Kienle, R. Zeller, R. Frahm, Z. Phys. B75, 495 (1989).
- 15 G. Schütz, M. Knülle, R. Wienke, W. Wilhelm, W. Wagner, P. Kienle, R. Frahm, Z. Phys. B73, 67 (1988).
- 16 R. Wienke, J. Pflüger, W. Wilhelm, G. Schütz, R. Frahm, to be published

Figure Captions

- Fig. 1 Principle of the magnetic array.
- Fig. 2 Measured vertical magnetic field of the asymmetric magnet structure and the derived first and second field integral along the symmetry axis. For definitions see eq. 1 and 2.
- Fig. 3 $B(\theta)$ plot of the central period.
- Fig. 4 Total brightness ($I'_R + I'_L$) calculated from the measured magnetic field at 10 keV as a function of horizontal and vertical angle. The angular range is $-1.5 < \theta_{hor} < 1.5$ mrad; $-0.2 \leq \theta_{ver} \leq 0.2$ mrad. A perfect electron beam with no divergence is assumed.
- Fig. 5 Circular polarized brightness ($I'_R - I'_L$) for the same parameters as in Fig. 4.
- Fig. 6 Degree of circular polarization $(I'_R - I'_L)/(I'_R + I'_L)$ for the same parameters as in Fig. 4. Values at the largest horizontal angles were set to zero since the intensities needed to calculate the polarization become very small and inaccurate.
- Fig. 7 Schematic drawing of the existing W1 beamline.
- Fig. 8 Total flux at 7.243 keV through an aperture (2 x 1 mm) that is moved through the horizontal plane. Open circles represent measurements. The full line is a calculation. For details see text.
- Fig. 9 Degree of circular polarization at 11.564 keV as a function of the vertical angle. Measured values are shown by the open circles. Also a representative error bar is shown.
- Fig. 10 Degree of circular polarization at 7.243 keV as a function of horizontal angle at a 0.16 mrad vertical angle. Only the central region is strongly polarized.



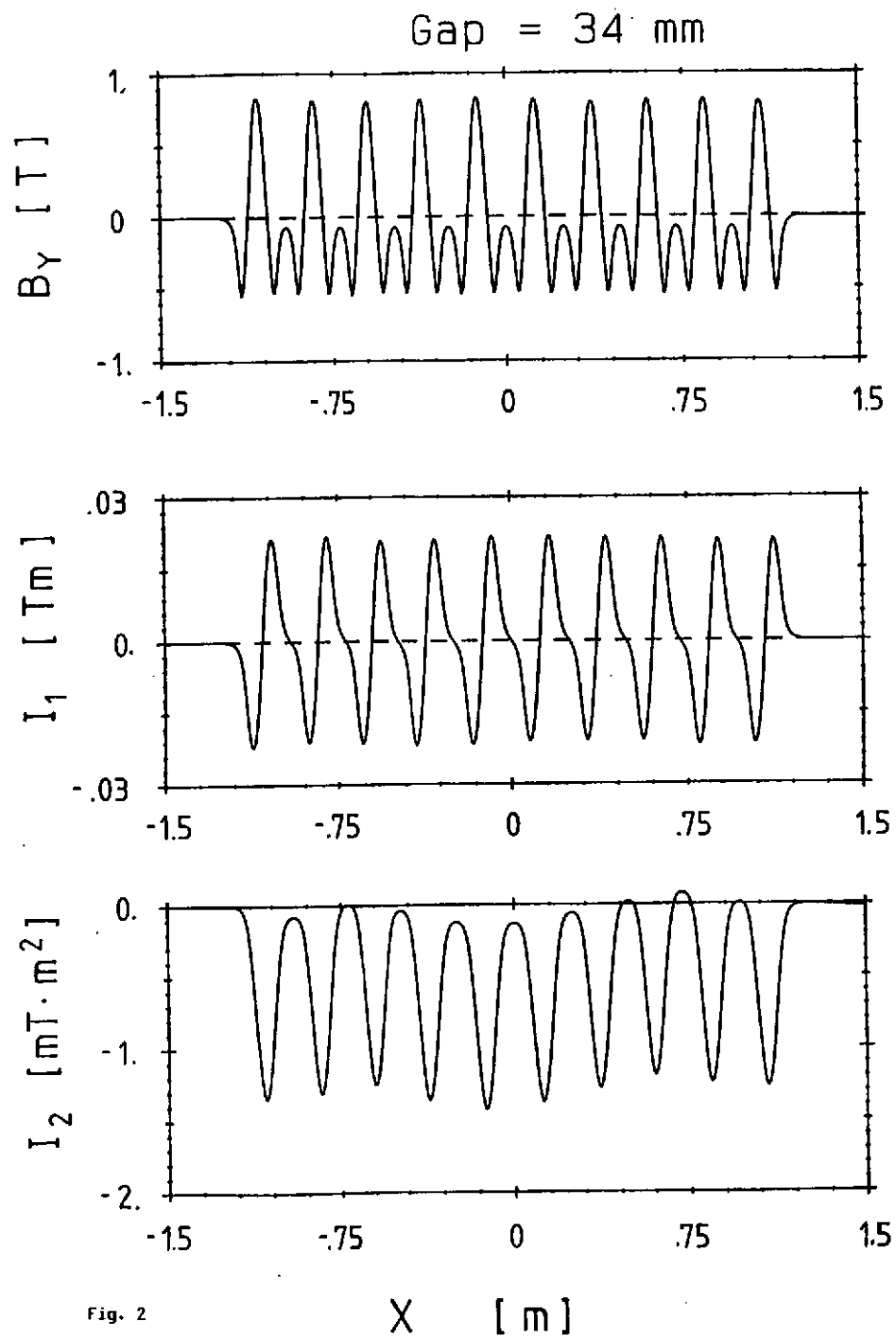


Fig. 2

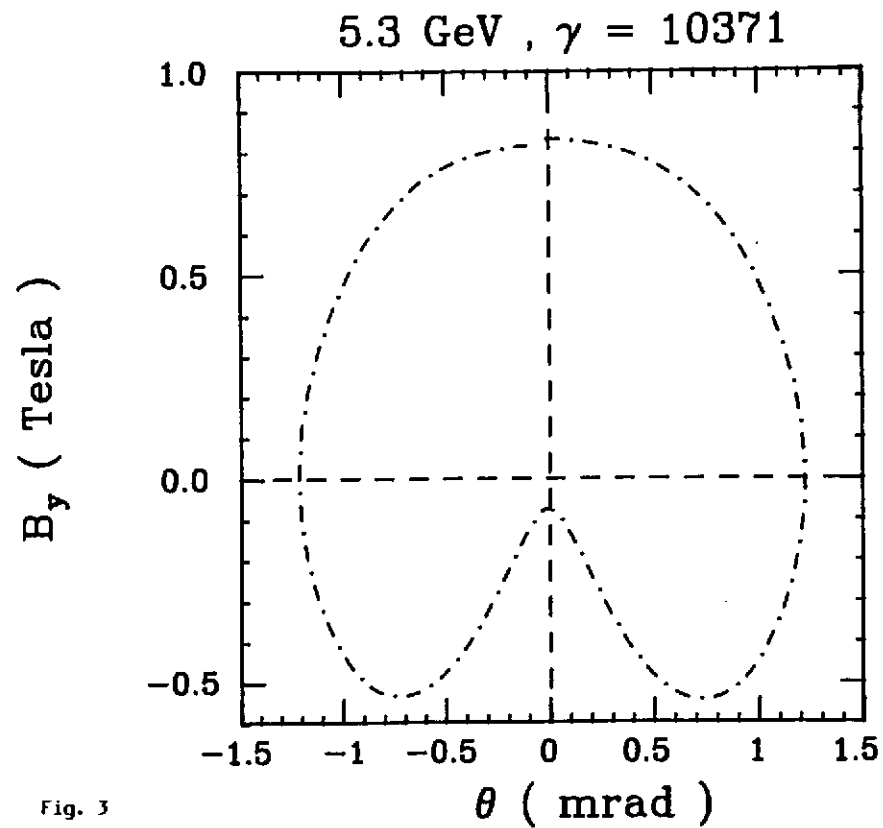


Fig. 3

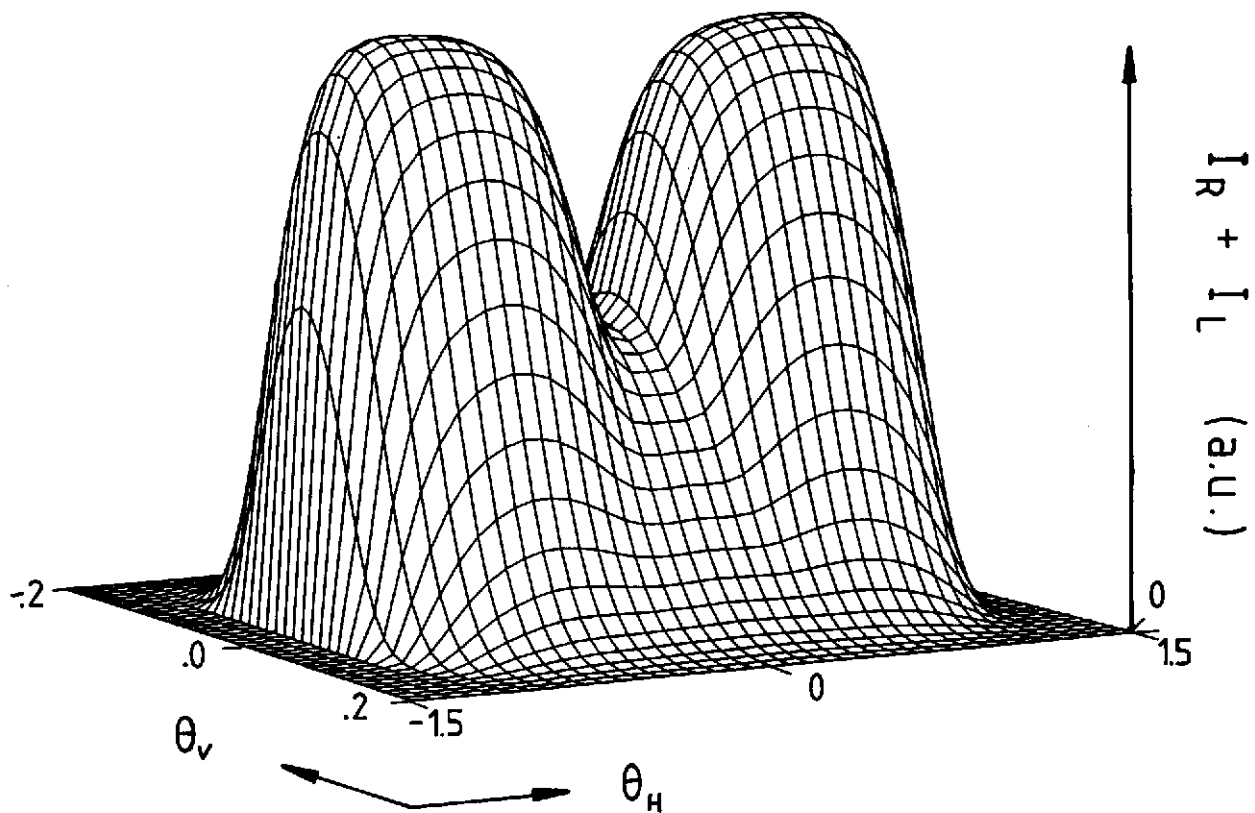


Fig. 4

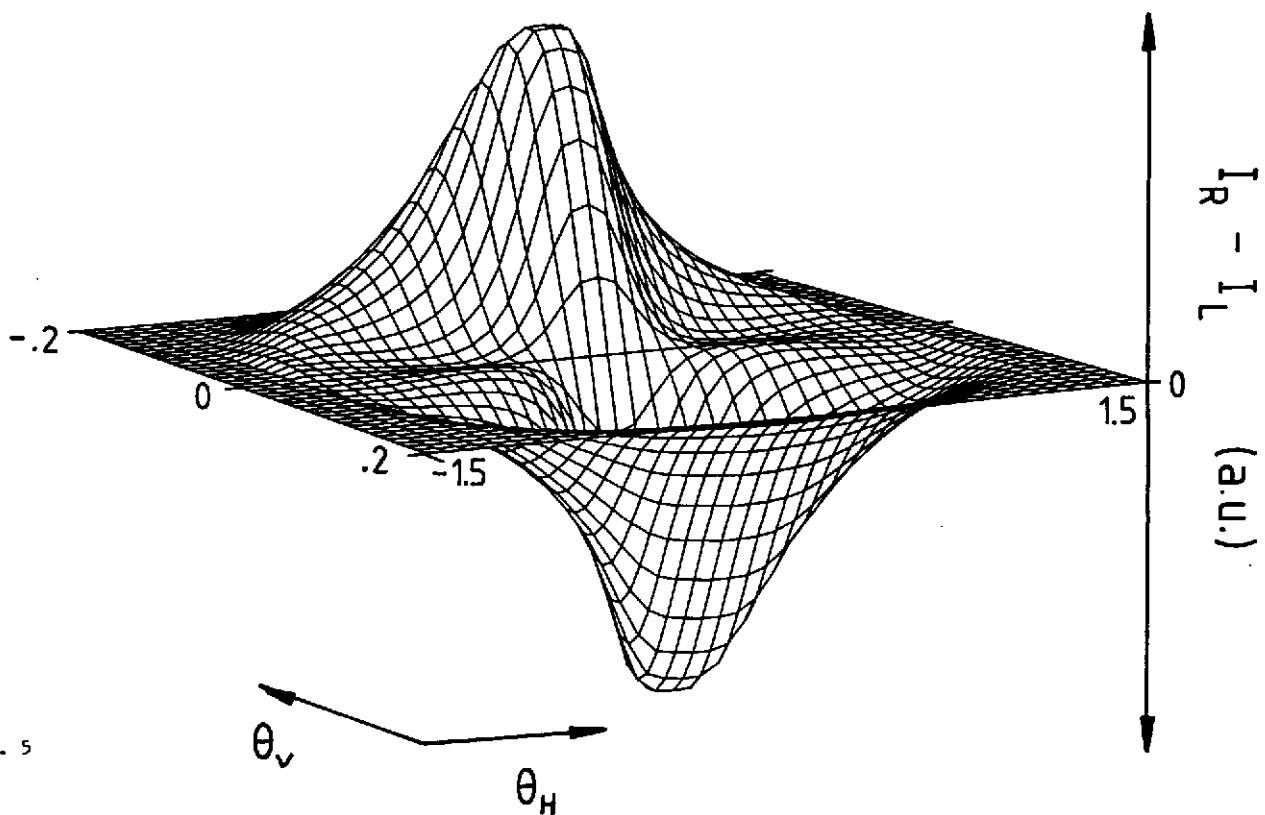


Fig. 5

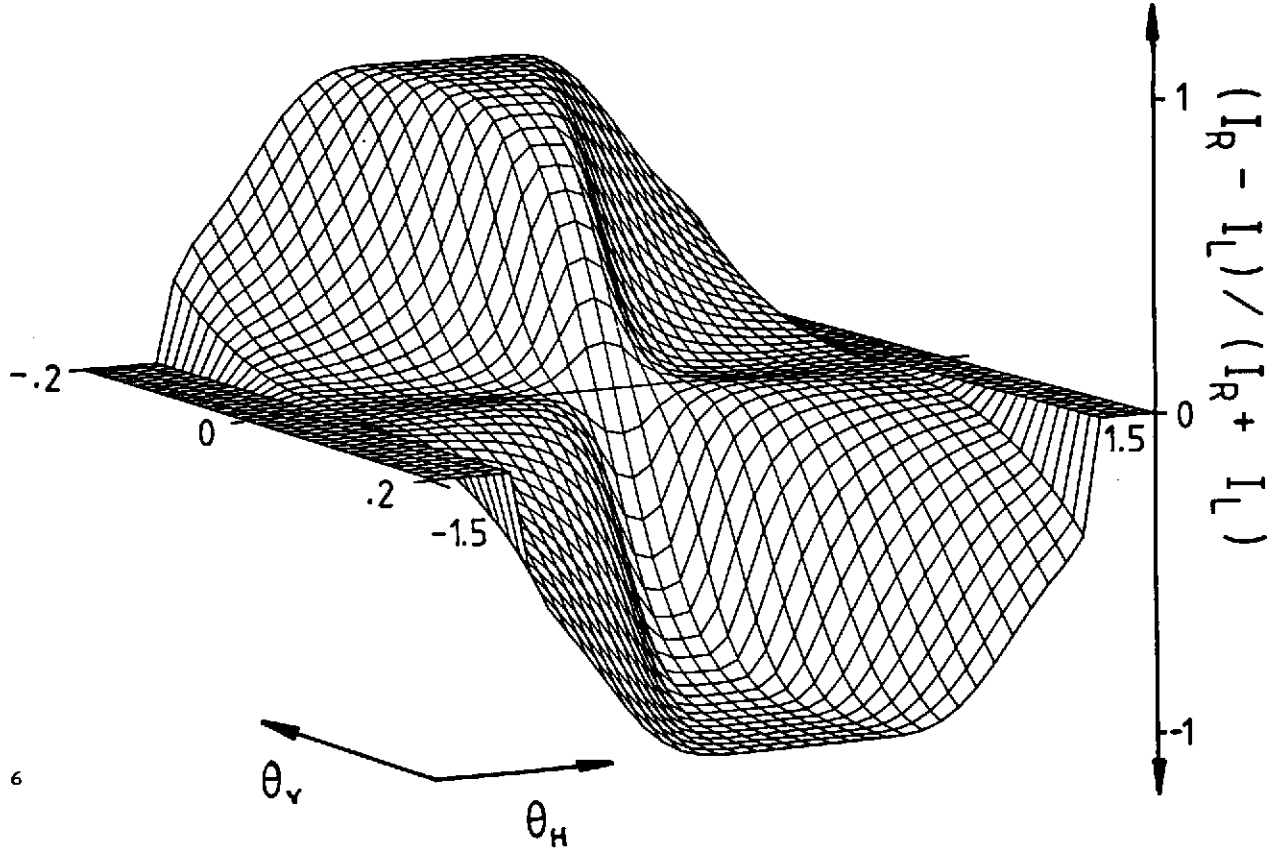


Fig. 6

W1 Beamline

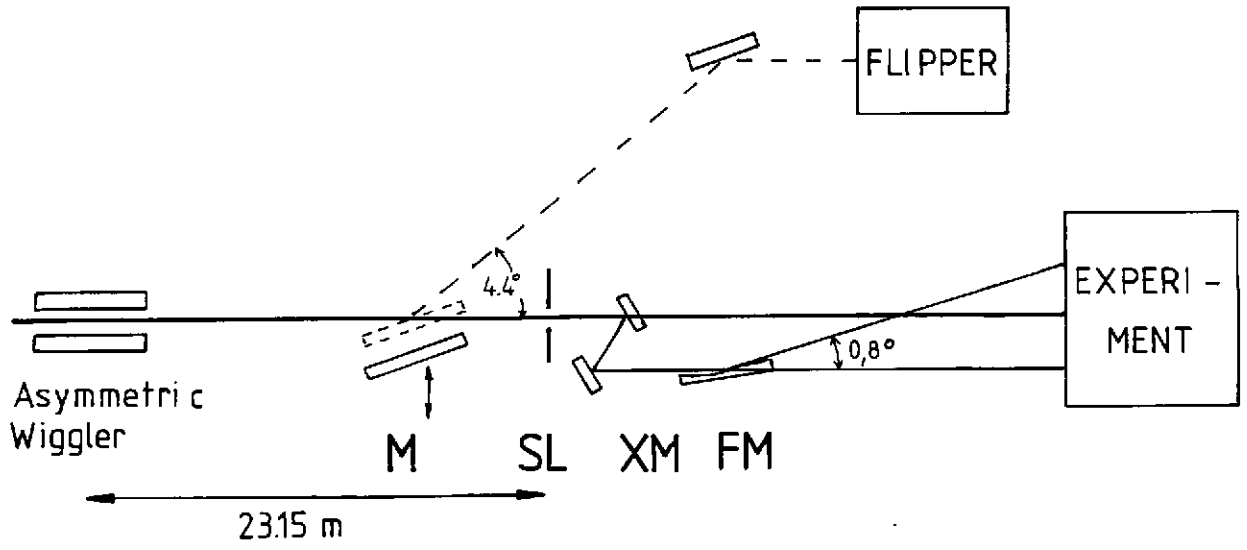


Fig. 7

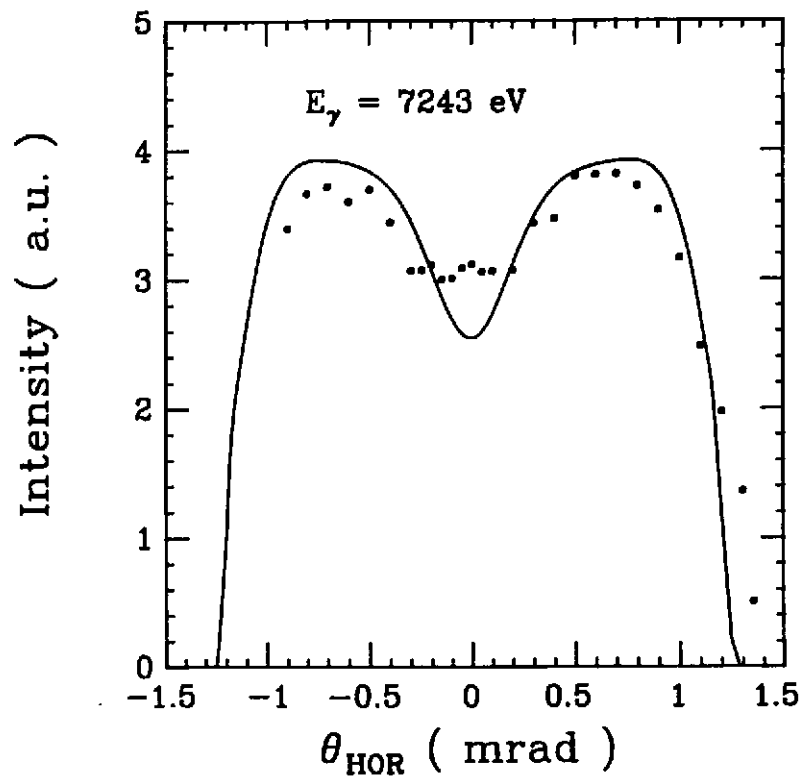


Fig. 8

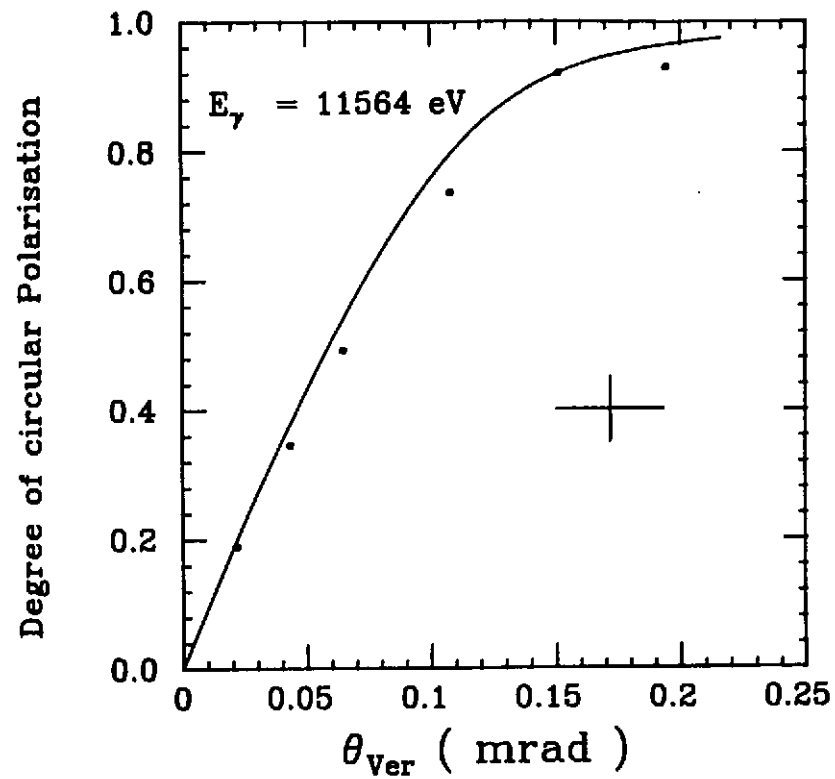


Fig. 9

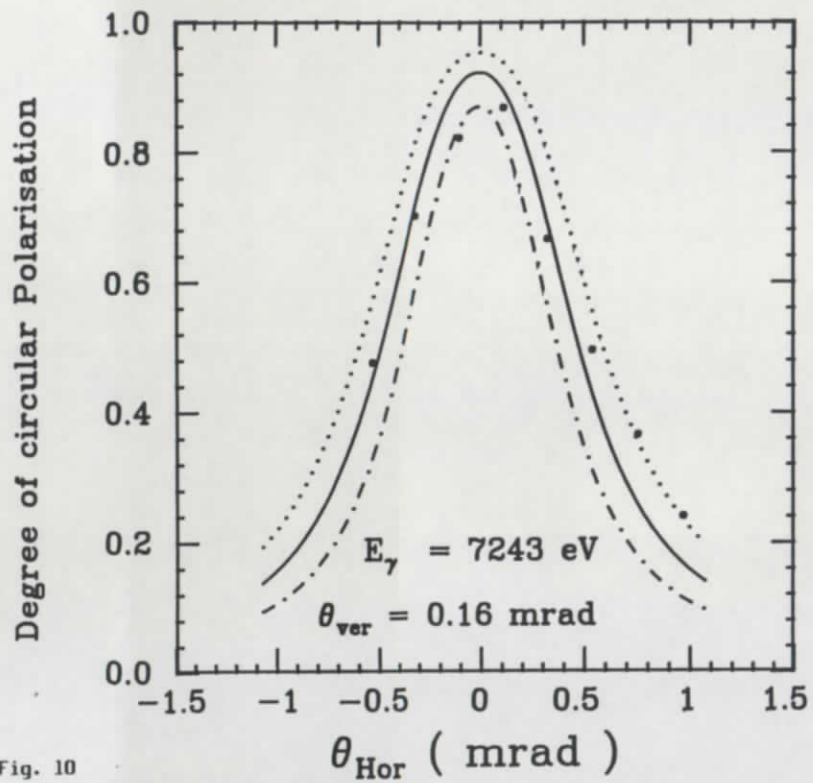


Fig. 10

